AIAA JOURNAL
Vol. 32, No. 3, March 1994

Mixing Enhancement by and Noise Characteristics of Streamwise Vortices in an Air Jet

C. B. Rogers*
Tufts University, Medford, Massachusetts 02155
and
D. E. Parekh†
McDonnell Douglas Research Laboratories, Saint Louis, Missouri 63166

Streamwise vortices are generated in the exit of a Mach-0.6 rectangular air jet by half-delta wings at various angles of attack. They entrain close to 50% more mass by 3.7 jet diameters and reduce the downstream jet noise at 23 diameters away from the jet nozzle by up to 3 dB. The mixing improvement and jet noise characteristics are both strong functions of the strength and relative position of the vortices. Mass entrainment measurements were measured quantitatively with local pitot-static pressure measurements and through image analysis. The image analysis also gave average spatial information about the mass entrainment through scalar transport. The results of the acoustic analysis showed that the vortex generators tended to reduce low-frequency noise and introduce high-frequency noise, resulting in noise reduction downstream of the nozzle and an increase in the noise normal to the jet flow. Additionally, as Mach number increased, the downstream jet noise reduction increased.

Nomenclature

D = major diameter of nozzle
d = minor diameter of nozzle
d_h = hydraulic diameter of nozzle
M = Mach number
$\dot{m}$ = mass flow rate
St = Strouhal number
s = distance between generators
U = local mean streamwise velocity
U_0 = jet exit mean streamwise velocity
x = streamwise coordinate
y = spanwise coordinate
z = normal coordinate
η = mixing effectiveness
θ = polar angle relative to jet centerline
ϕ = azimuthal angle relative to nozzle major axis

Introduction

THE mixing and acoustic characteristics of jets are of great importance to both the industrial and academic communities. Thorough mixing of a jet of fuel with its surroundings is important in the combustion process. Jet noise considerations can drive the development of commercial aircraft propulsion systems and determine an aircraft's ability to meet government environmental regulations. For both mixing and noise, the jet shear layer plays a dominant role. Thus, researchers have concentrated much attention on controlling the behavior of free shear flows.

Numerous passive and active techniques for controlling jet mixing have been demonstrated. Elliptic[1] and indeterminate origin[2] nozzles illustrate how changing nozzle cross-sectional shape or trailing-edge contour can significantly enhance mixing. Illustrations of mixing enhancement by active excitation include bifurcating and blooming jets[3,4] and amplitude modulated piezoelectric excitation of jet flows.[5] A full listing of the various mixing enhancement approaches would easily number over a hundred references.

Received Nov. 25, 1992; revision received Aug. 9, 1993; accepted for publication Aug. 11, 1993.

*Assistant Professor, Department of Mechanical Engineering. Member AIAA.
†Scientist, McDonnell Douglas Aerospace. Member AIAA.

One subcategory of mixing enhancement approaches employs streamwise vorticity. The lobed mixer, for example, introduces streamwise vorticity through skewed mixing layers generated by a lobed interface between primary and secondary flows.[6] Rectangular and triangular tabs protruding into a jet at the nozzle exit enhance mixing in subsonic and supersonic flows.[7,8] Each tab generates a counter-rotating pair of vortices with the common flow direction between the vortices determined by the inclination of the tab.[9] Tabs can additionally reduce noise through enhanced mixing in subsonic flows[10] or through screech reduction in supersonic flows.[11] Tabs have also been observed by several investigators to reduce noise at low frequencies while increasing noise at high frequencies.

Practical considerations typically, though not always, favor simple, passive approaches to mixing enhancement and noise control. Additionally, many different approaches to mixing enhancement involve the generation of secondary vorticity, making an understanding of the interaction of streamwise vorticity with a jet shear layer relevant to many techniques. For these two reasons, we have focused on the effect of streamwise vortices on the mixing and acoustic characteristics of jet flows.

This research adds to the existing body of literature in several ways. First, to systematically study the effect of streamwise vorticity on jet behavior, we use half-delta-wing vortex generators. Unlike tabs, half-delta-wing generators provide direct control of the position, strength, and direction of rotation of each streamwise vortex. Second, we have sought to quantify the mixing effectiveness of streamwise vortices through an efficient image-processing approach. Third, this paper considers rectangular rather than axisymmetric jets. The work discussed here is one part of a larger study of artificially generated streamwise vortices in subsonic and supersonic, round and rectangular jets. Other topics currently under investigation include the effect of streamwise vortices on ejector performance, alternative methods of generating streamwise vortices, and thrust losses associated with vortex generator devices.

Experimental Design and Methods

Experimental Setup

All measurements were taken on a transonic air jet in an anechoic chamber. Air entered a 30.5-cm diameter plenum from a set of compressed air tanks. This air source could continuously supply the desired mass flux for these experiments so no "blow-down" mode was necessary. The nozzle pressure ratio is actively

controlled using a set of computer-controlled solenoid valves of various sizes. By monitoring the nozzle pressure ratio, and controlling the valves accordingly, the computer maintained the target jet velocity to within ±0.5%.

Downstream of the plenum, the air passed through a honeycomb, a series of fine mesh screens and then a round-to-rectangular contraction (9:1 area ratio) before exiting a rectangular nozzle extension. The 2:1 rectangular nozzle extension (6.35 cm × 12.7 cm) has two sets of five holes on the top and the bottom that allowed us to vary the generator spacing and the development length, the distance between the generator and jet exit (see Fig. 1). The hole patterns on top and bottom were identical, and both rows of hole patterns were symmetric about the center. The row closer to the exit had a spacing of 20% of the major axis (1.27 cm), and the row farther back had a spacing of 30% of the major axis (1.875 cm). The walls of the nozzle were made of Plexiglas on the top and bottom and aluminum on the sides. The contraction and nozzle could be rotated about the jet axis to investigate different azimuthal planes.

We used three different generators of varying size and leading-edge sweep angle and installed them in different combinations of position and angle of attack (Fig. 2). Previous research[12] shows a strong effect of generator sweep angle and angle of attack on vortex bursting. Although a burst vortex does not have the same high rotational speed core of the unburst vortex, the burst phenomenon itself would be expected to enhance mixing locally. Thus, the generator parameters were chosen to span both burst and unburst cases.

Measurement Techniques

Mixing and Velocity Measurements

To measure the mixing, we used a combination of flow visualization and image-processing techniques. The mixing was illuminated by a 20-W copper-vapor laser sheet about 150-mm wide and 1-mm thick. The sheet was traversed parallel to the jet centerline, allowing us to visualize the growth of the jet (see Fig. 3). It should be noted that, unlike an argon-ion laser, the beam of a copper-vapor laser has a top-hat intensity profile, and therefore one sees roughly a uniform light intensity in the laser sheet, except at the edges of the laser sheet. The best visualization resulted from filling the test cell with smoke from a ROSCO 1500 fog machine and then blowing clean air through the jet. By videotaping the light reflected off the smoke particles using a Panasonic charge-coupled device (CCD) camera (model Digital-5000) and a Sony BetaCam (model 750) recorder, we were able to get images of the jet dispersion and mixing at numerous locations downstream of the jet exit. The camera and light source were adjusted to avoid saturating the CCD (maximum pixel value at 230).

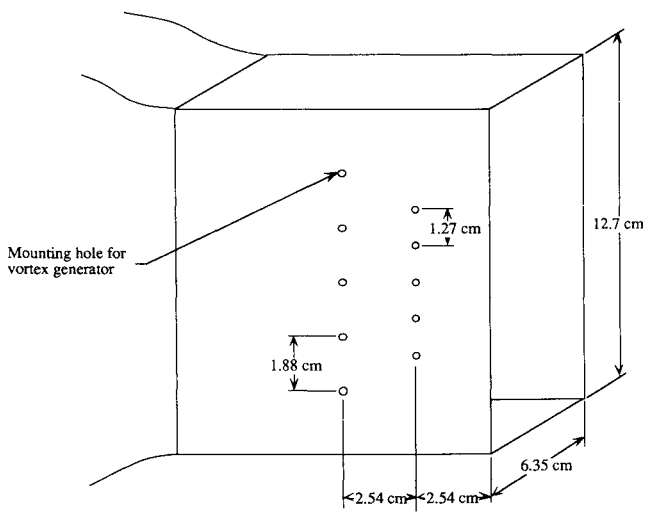

Fig. 1 Schematic of rectangular nozzle extension.

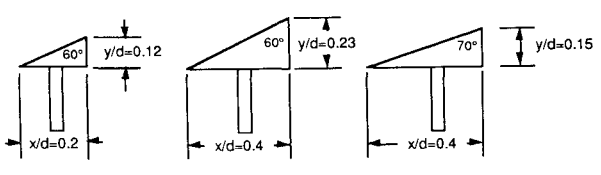

Fig. 2 Half-delta-wing vortex generators.

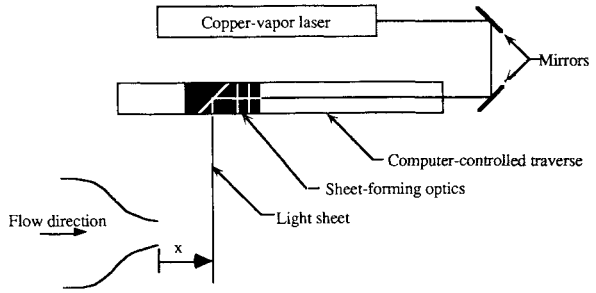

Fig. 3 Schematic of laser light sheet delivery system.

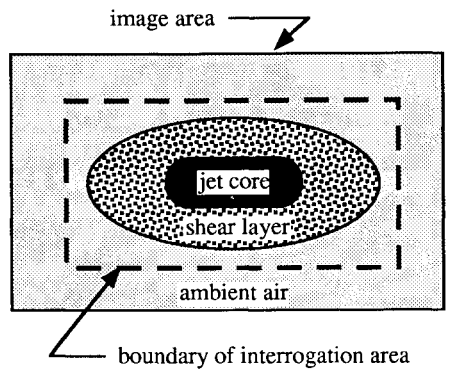

Fig. 4 Schematic representation of image interrogation area.

Using a Macintosh IIx, equipped with TrueVisions NuVista video interface; we were able to make quantitative measurements of the local smoke concentration and therefore the mixing effectiveness. Since the pulse rate of the laser is 10 kHz and the pulse duration is 30 ns, each video frame corresponds to an average of approximately 330 instantaneous images over a 0.033-s period. This implies, for a Mach number of 0.6, that the smoke concentrations are averaged over a jet column length of $l/d_h \sim 80$. It is therefore important to note that these measurements are not measurements of molecular mixing but rather measurements of both mixing and large-scale unsteadiness. This problem can be reduced using high-speed video or shuttering the laser sheet.

Assuming that each smoke particle tags a volume of fluid, one can estimate the volume of entrained fluid at any location in the jet from the smoke concentration. Assuming that the fog (smoke) droplets are relatively uniform in their ability to scatter light, that is, roughly the same size and shape, the local measured light intensity should vary linearly with the local smoke concentration. Hence, the local pixel value should correspond to the local concentration of smoke and therefore the volume of ambient fluid, assuming that the light does not saturate the CCD array and that the response of the CCD varies linearly with light intensity. Therefore by examining the difference between two images, one can see where the vortex generators entrained more ambient fluid than did the reference case of no generators.

We define a mixing effectiveness, or efficiency, by comparing the average smoke concentration (or pixel values) inside an interrogation area A to the average pixel value outside the interrogation area, that is,

$$\eta \equiv \frac{\text{avg}\langle \text{pixel values within } A\rangle}{\text{avg}\langle \text{pixel values outside } A\rangle} \approx \frac{\text{droplets entrained}}{\text{ambient droplet density}} \quad (1)$$

This effectiveness therefore roughly compares the number of smoke particles inside a predefined region of the image to the

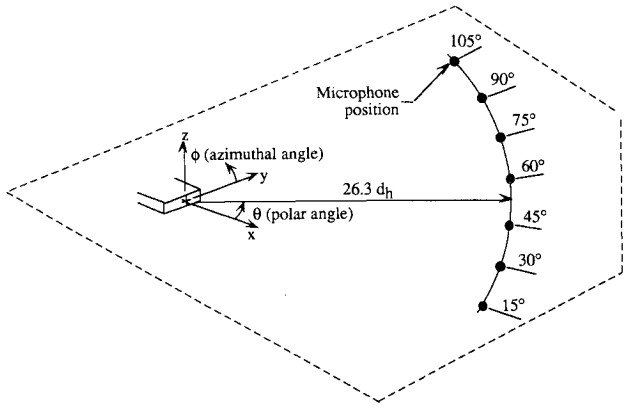

Fig. 5 Schematic of microphone layout.

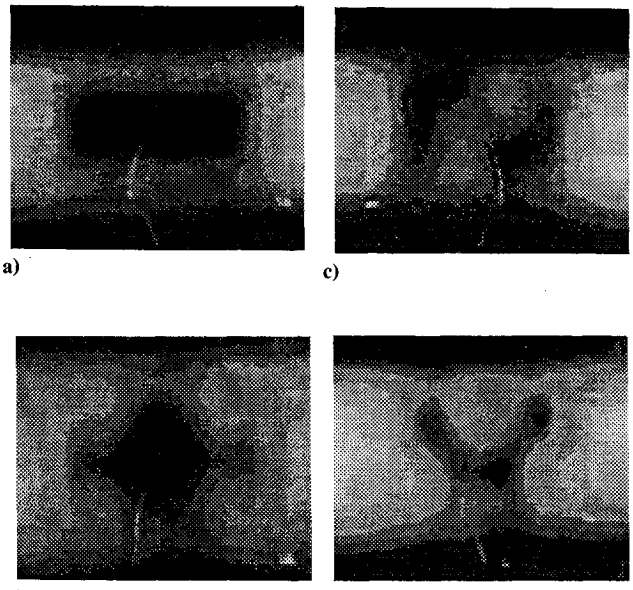

Fig. 6 Laser light-sheet visualization of jet mixing patterns at x/d_h = 3.7 and M = 0.6.

number of smoke particles in the ambient air. The interrogation area is a rectangular region in the cross-sectional image that surrounds the jet core, the shear layer, and a small amount of ambient fluid as shown in Fig. 4. The size and relative position of the interrogation area are the same for all cases. It should be noted that we are using this effectiveness only to look at trends in mass entrainment, this is not a rigorous quantitative method of measuring the mass entrainment.

One difficulty in the setup is that, to make accurate measurements of smoke concentration using the reflected light, one must insure that the intensity of the incident light is uniform throughout the interrogation domain. The variation in the reflected light intensity on either side of the jet was within 2%. Again, since the light intensity of a copper-vapor beam has a top-hat profile, one would expect the same pixel value everywhere outside of the jet but in the interrogation domain. This indicates that the ambient air was uniformly seeded and that a small percentage of the laser light was either scattered or absorbed as it passed through this domain. This uniformity also implies that the CCD array is uniform in its response to light, and hence we did not need to calibrate individual CCD elements.

After evaluating a large number of configurations, we found three different configurations that clearly demonstrated mixing control. We compared the amount of mixing in each of these cases at a number of locations downstream of the jet exit. We also used a pitot-static probe to measure the mean velocity profile of the jet. The probe was mounted on a computer-controlled, three-dimensional traverse. Profiles were taken both along the geometric centerline of the jet and in planes perpendicular to the streamwise direction. We compared the mixing effectiveness values determined from the images with the mass entrainment values computed from velocity profiles. The camera was set at 10 deg off the geometric centerline of the jet due to stability issues.

Acoustic Measurements

We used an array of seven Brüel and Kjaer Model 4135 condenser microphones to investigate the acoustic field (see Fig. 5). These microphones were placed at 15-deg intervals from 15 to 105 deg off the jet centerline at a distance of 26.3 d_h from the center of the nozzle. Full acoustic spectra were taken at each of these microphone locations at azimuthal angles of 0, 30, 60, and 90 deg. These measurements were made by rotating the contraction and nozzle and keeping the microphones stationary. The microphones were calibrated daily with a B & K Pistonphone. The Sonex 10-cm-thick sound-absorbing foam covers all of the surfaces of the test cell, which is 4.9-m square × 3.7-m tall. The Sonex foam has an absorption coefficient above 0.99 for frequencies above 500 Hz, above 0.9 for frequencies above 350 Hz, and above 0.7 for frequencies above 250 Hz.

All of the microphone signals were conditioned with a low-pass filter at 23 kHz and sampled at 51.2 kHz with a Preston 13-bit analog-to-digital converter. A DEC VAXlab computer calculated the final spectra from an average of 32 2048-point fast Fourier transform (FFT) operations on each signal windowed with a Hanning function. This provides a frequency resolution of 25 Hz. The spectral data were digitally high-pass filtered at 250 Hz before computation of the overall sound pressure level (OASPL) to minimize the effect of the non-anechoic characteristics of the test cell at low frequencies.

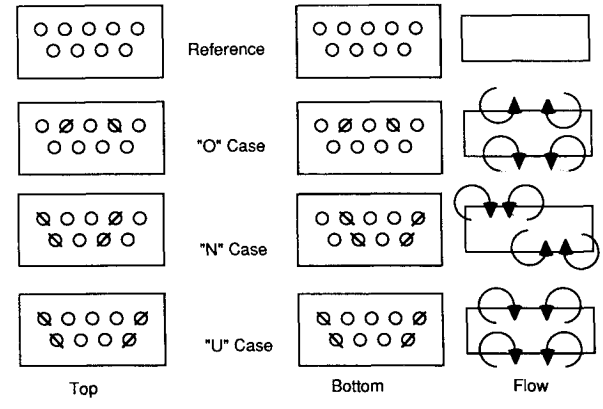

Fig. 7 Schematic of vortex generator configurations as viewed from top of nozzle. Note that generators are drawn schematically at 45-deg angle of attack but were actually at 20 deg. See Fig. 1 for flow orientation.

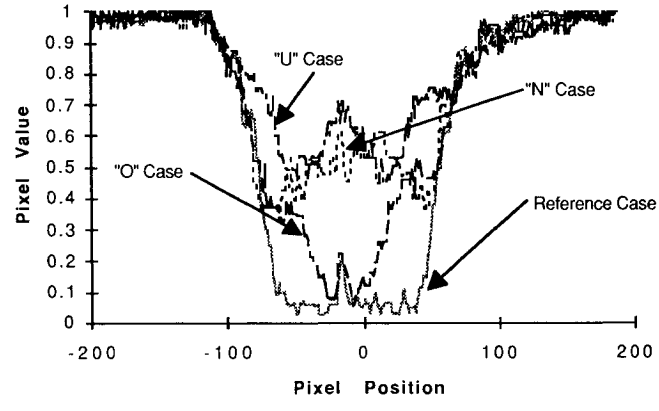

Fig. 8 Normalized pixel values across the jet centerline for cases in Fig. 6.

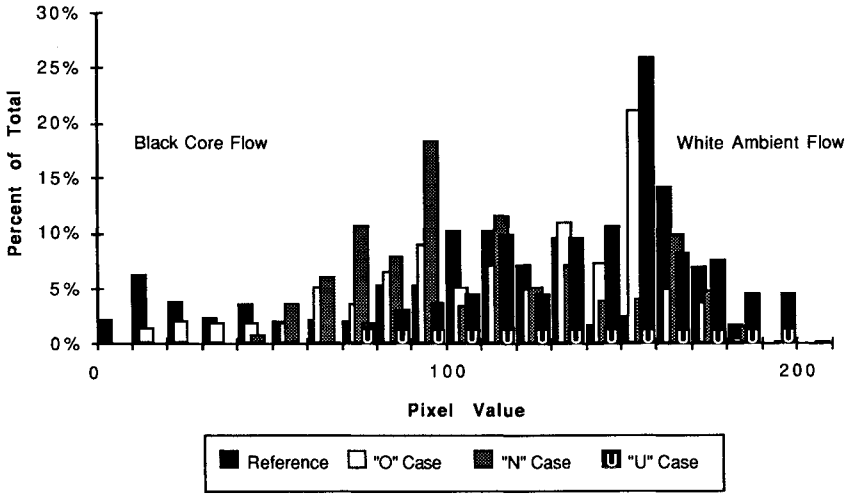

Fig. 9 Normalized histograms of interrogated area.

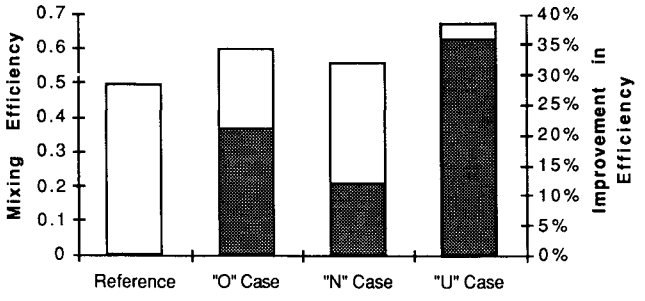

Fig. 10 Mixing effectiveness measurements {$[(\eta/\eta_{ref})-1]$ is in gray}.

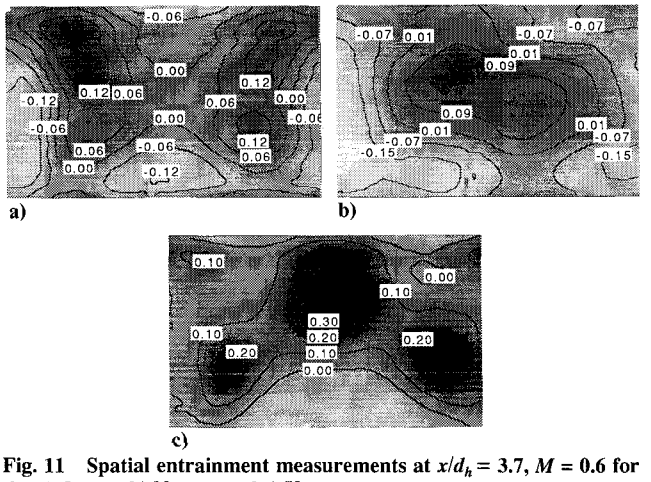

Fig. 11 Spatial entrainment measurements at $x/d_h = 3.7$, $M = 0.6$ for the a) O case, b) N case, and c) U case.

Measurement Uncertainty

There is a high measurement uncertainty in the optical mixing effectiveness measurements. The effects of varying interrogated domains, effects of finite laser sheet thickness, and uncertainty in the image digitization process all affect the final measurement. In the present study, the finite width of the laser sheet was the largest source of uncertainty. Because of room limitations, we were unable to accurately resolve the ambient air above and below the nozzle. After varying each of these parameters, we estimate a conservative uncertainty of close to 20%. The large uncertainty prohibits the use of this technique as a rigorous quantitative method for measuring mass entrainment. This includes both spatial variations and linearity of the CCD array. However, relative variations have a much lower uncertainty, implying that the images can give a quantitative spatial comparison between the various runs. To minimize errors, all images were normalized by the "no-flow" case to reduce the effects of the decrease in laser light intensity at the edges of the laser sheet. The no-flow case is simply the same image with no jet flow.

Mean velocity measurements have less than 2% uncertainty for flow angles under 30 deg. Uncertainty in the calculation of the local density ρ is approximately ±2%, based on estimates of density variations across the jet exit using the one-dimensional, compressible, isentropic flow equations.

Based on experimental error and multiple measurements of identical cases, we estimate the accuracy and repeatability of the acoustic measurements to be within ±1 dB for the frequency range of 20–10 kHz. Frequencies higher than 10 kHz did not make a significant contribution to the OASPL.

Results

Mixing Results

We examined over 40 different configurations, with a representative set of entrainment patterns shown in Fig. 6. These particular pictures were taken at 3.7 hydraulic diameters downstream of the jet exit at a speed of 200 m/s ($M = 0.6$). The first picture (Fig. 6a) is the reference case of the jet without vortex generators. It shows how the shape of the exit geometry is retained downstream. The white sections on either side of the picture correspond to the smoke-laden ambient air, and the black core reflects the clean core flow of the jet. The varying shades of gray reflect the ambient air being entrained into the shear layer. Again, since each picture is a temporal average of 0.033 s, the resulting pictures show entrainment resulting from both flow unsteadiness and vortex mixing. All measurements are time-averaged entrainment measurements. One should also note that, due to the finite laser sheet thickness, the light intensity drops off at the edges.

All three other pictures (Fig. 6b–6d) have one set of vortex pairs on top and bottom. In the case of the second picture (Fig. 6b), the vortex pairs are formed by two generators, with the common flow away from the jet centerline. One can see that the vortex pairs tend to move the high-speed core flow out along the vertical axis while bringing in slow ambient fluid along the horizontal axis. Figure 6c shows the effect of asymmetry by having the common flow of the top pair be offset laterally from the common flow of the bottom pair. Both pairs have a common flow into the center of the jet in this case. Finally, Fig. 6d shows the best mixing case, where the vortex pair on the top has a common flow toward the jet centerline and the generators on the bottom have a common flow away from the jet centerline. These cases will be referred to as the "reference" case, the "O" case, the "N" case, and the "U" case, respectively, reflecting the apparent shape of the core flow.

Figure 7 shows the actual placement of the generators for all three cases. Note that cases N and U adopt generator stacking in which one generator is placed behind another so that two genera-

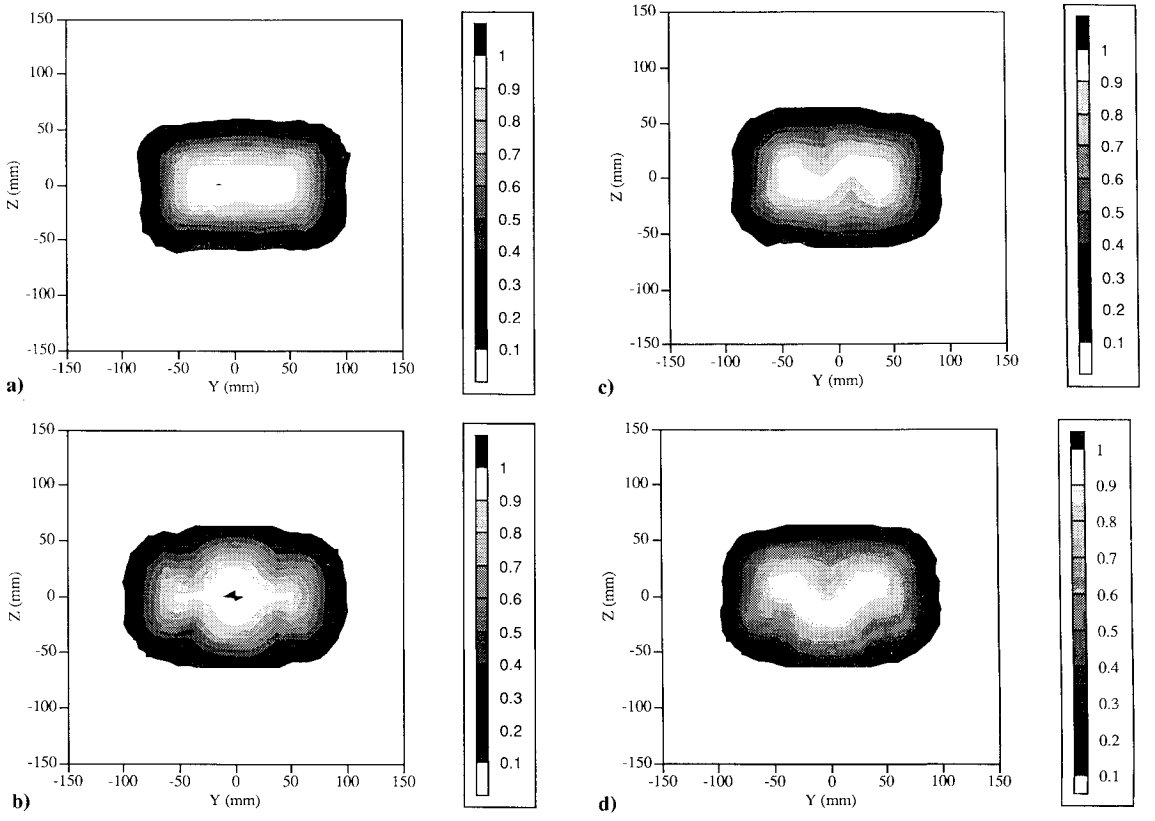

Fig. 12 Normalized velocity contours (U/U_0) at $x/d_h = 3.7$ and $M = 0.6$ for the a) reference case, b) O case, c) N case, and d) U case.

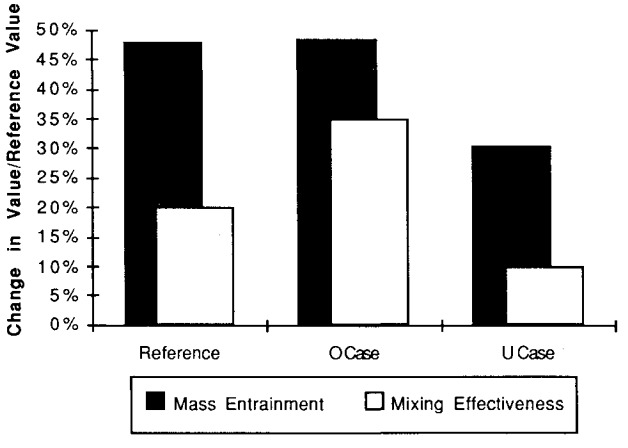

Fig. 13 Comparison of integral measurements.

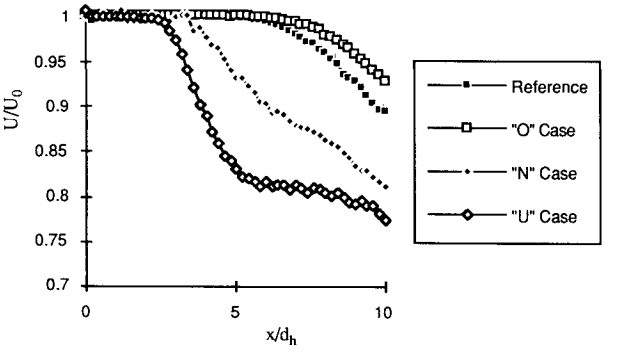

Fig. 14 Comparison of centerline velocity decay profiles.

tors produce each vortex. From these pictures, one can clearly see the effect of the direction of the common flow between the generators. In the last picture, for instance, the vortex on the bottom left tends to pull in slow ambient flow from the side of the jet and push the fast core flow out the bottom of the jet. Likewise, the vortex on the top tends to pull slow flow in from the top and expel fast core flow out the side. By varying the placement of these generators, we can create almost any pattern.

Figure 8 compares the pixel values (or entrained mass of smoke) along the geometric horizontal centerline of each picture (Fig. 6), normalized by the pixel value of the ambient air off to the side. The normalization reduced effects of variation in laser power and variations in seeding. Although there is considerable scatter in the results, the trends are evident. First, the plot clearly shows that the light intensity on either side of the jet does not vary by more than 2%. That is, the smoke concentration in the room is uniform and the laser light absorbed by the smoke particles is negligible. Second, the O and N cases show little variation in the mixing in the shear layer but show enhanced mixing in the core. This is evidenced by the similarity in the slope of the concentration at the edges of the jet. The change in slope of the U case comes from the fact that the jet center has moved off the geometric centerline. The N case appears to be almost as effective at mixing as the U case in the jet core, with the O case lagging somewhat behind. This is really true only along the geometric centerline as most of the entrainment in the U case was above the centerline. The small sharp peak near the jet center is a result of the light reflected off a piece of tubing and therefore can be disregarded.

Since none of the profiles are axisymmetric, the single line plot tells little about the overall mixing effectiveness, and therefore a more general histogram would be more useful. Figure 9 is a histogram of pixel values within the interrogated area. Low pixel values correspond to the unseeded core flow, and high pixel values correspond to the ambient seeded areas. The region in between reflects the mixing of the two areas. Figure 9 shows both the U and the O case having far more white pixels (i.e., better mixed regions) than the other two cases. The N case has a peak in the midrange and the reference case has a relatively even distribution. Note that both the N and the U cases have essentially no "black" core flow.

Figure 10 shows the mixing effectiveness for each of the cases listed earlier. The white bars reflect the actual mixing effective-

ness, and the gray bars show the percent improvement of each case over the reference case. The results agree with the images in Fig. 6, showing almost a 40% improvement in the U case. The O case still shows considerable improvement, whereas the N case shows only a modest improvement (about 10%). This low value for N is most likely a result of the finite laser sheet width. Thus, the addition of strategically placed vortex generators can significantly increase mixing in a jet. The results also show that the placement of these generators has a large effect on the mixing enhancement, since both the N and the U cases have the same number of vortex generators in the flow.

In fact, careful examination of the images gives some insight into the spatial variation in mass entrainment. Figure 11 shows the difference between the three cases and the reference case. Positive numbers (black) imply more entrainment than the reference case. Looking first at Fig. 11a, one can see symmetry due to the two vortex pairs. The vortex pairs entrain ambient fluid from the side into the core and move core fluid out top and bottom. Hence, one sees an increase in entrainment to the two sides of the core but a slight decrease above and below the core. The asymmetry in the vertical is most likely a result of the finite laser sheet thickness. Figure 11b demonstrates the effect of asymmetrical placement of the vortex pairs. The image shows an increase in the entrainment in the core but shows substantial decreases on the top and bottom of the picture. Again, this is probably a strong function of the finite laser sheet thickness. Finally, Fig. 11c shows the increase in entrainment of the U case. This case has the largest increase in entrainment, with a peak just above the geometric centerline of the jet. This peak results from the vortex pair on the top pumping ambient air into the jet core. The pair on the bottom pumps the jet flow out away from the centerline, implying a real gain in entrainment below the jet center. The two peaks off to the side are indicative of the ambient flow being pumped in by the lower vortex pair. Thus, Fig. 11 shows that placement of the generators has a large effect on the spatial mass entrainment. In the asymmetric case (N), the vortices seem to impede each other, whereas in the U case there is a clear pumping direction (down), and hence we find the most effective mixing.

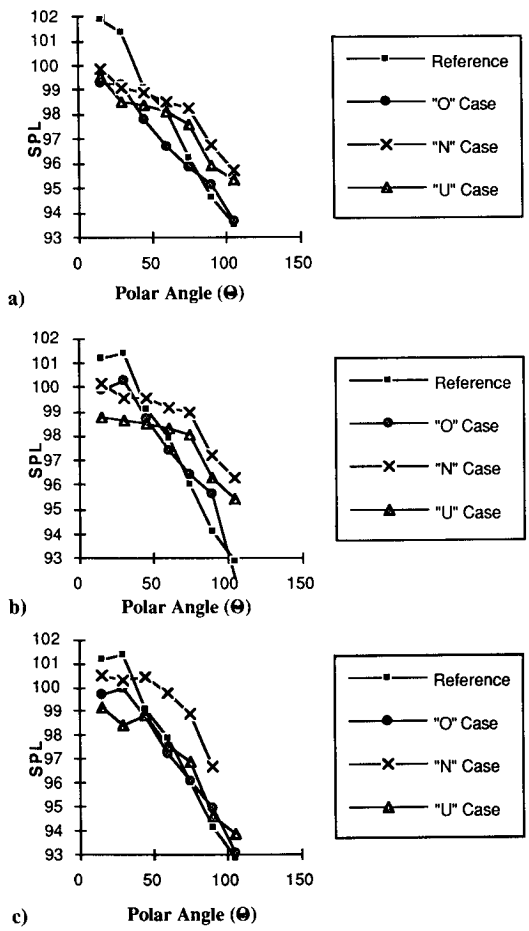

Fig. 15 Effect of mixing pattern on OASPL directivity for a) $\phi = 0$ deg, b) $\phi = 45$ deg, and c) $\phi = 90$ deg.

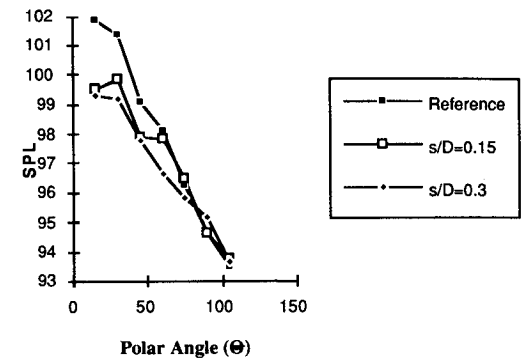

Fig. 16 Effect of generator spacing on jet noise.

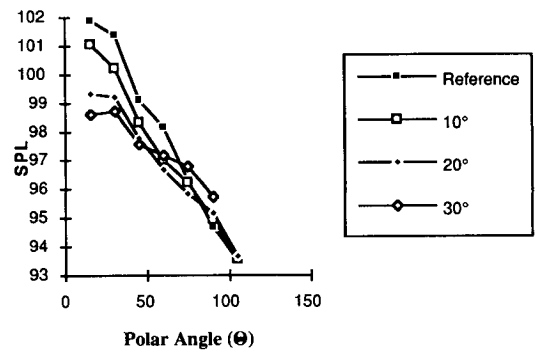

Fig. 17 Effect of generator angle of attack on jet noise.

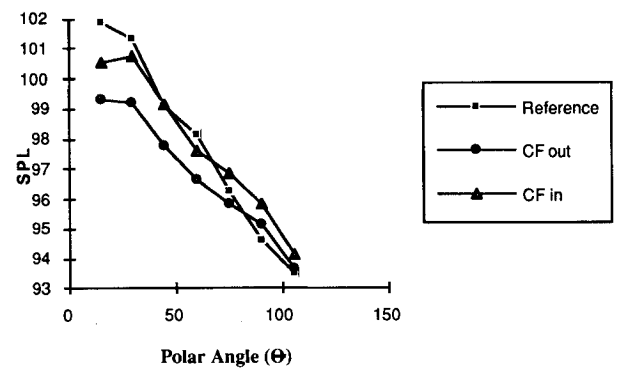

Fig. 18 Effect of common flow direction on jet noise at $\phi = 0$.

Velocity Results

The mean streamwise velocity contours (Fig. 12) look qualitatively very similar to the laser-illuminated images (Fig. 6). Since the scalar transport depends strongly on the jet velocity field, one would expect similar patterns. Figure 12 shows the velocity profiles for each of the four mixing cases at $x/d_h = 3.7$. The contour values correspond to normalized velocity values. All velocities are normalized by the exiting core velocity. One notices the same regions of slow ambient flows and fast core flows being manipulated by the streamwise vorticity as seen in the images.

From the image and velocity data, one can compare the mixing effectiveness as defined in Eq. (1) to a computed mass entrainment fraction as defined next:

$$\text{mass entrainment fraction} \equiv \frac{\int\int \rho U(x, y)\, dy\, dz}{(\rho_0 U_0 A)_{exit}} - 1 \qquad (2)$$

where the mass entrainment fraction is the ratio of the mass flow entrained to the mass flow leaving the jet nozzle. The local density is determined by using the one-dimensional isentropic equations and the local static to stagnation pressure ratio (measured by the pitot-static probe). Figure 13 displays the change in both integral measures normalized by the corresponding value for the reference case at $x/d_h = 3.7$. This comparison shows that the mixing effectiveness indeed follows the trends of the mass entrainment.

A commonly used indicator for mixing effectiveness is the centerline velocity decay profile. Figure 14 compares the centerline velocity profiles of each of the cases. In the N case, one sees a much faster centerline decay than in the reference case. In the O case, the vortices transform the core from a rectangular cross section to a circular shape having a larger characteristic diameter than the minor diameter of the reference rectangular core (Figs. 6 and 12). Thus, the centerline velocity in the O case decays more slowly than in the reference case. However, we have already seen in Fig. 13 that the O case is much more efficient at mixing and entrainment than the reference case. The U case centerline velocity decay is also somewhat misleading as the core center does not remain on the geometric centerline due to the asymmetric induced flow of the streamwise vortices. Thus, the centerline decay is, in fact, a very poor indicator of mixing for these types of flows.

Acoustic Results

As with the scalar and velocity fields, the streamwise vortices also alter the jet's acoustic field. We measured the acoustic characteristics of the jet for the four cases in Fig. 6 as a function of generator parameters and flow velocity. Because of room limitations the microphones were only at 23 diameters from the nozzle exit; hence the measurements were not true far-field measurements but should be indicative of the far-field noise characteristics. Further, the low-frequency measurements are affected by the room geometry. Figure 15 demonstrates the strong dependence that the acoustic field has on the fluid mixing pattern. The two cases with stacked generators (two generators per vortex) generate more noise normal to the streamwise direction yet still reduce the sound pressure level downstream. Figure 15 also shows the azimuthal variation of the sound field for the various cases. The U case shows the greatest variation with ϕ; the off-axis noise in that case decreases as ϕ increases from 0 to 90 deg. Finally, it should be noted that there is not typical peak in the sound pressure level (SPL) at $\Theta = 30$ deg in the $\phi = 0$ deg case, whereas the other two azimuthal angles (45 and 90 deg) both show the 15 and 30-deg microphones to be reading about the same amount of noise. This agrees with other work[13] which shows that peak at closer to 22.5 deg, with the SPL of 15 and 30 deg about equal for a Mach number of 0.6. The high SPL at the 15-deg microphone in the first case may be a result of pseudonoise.

In examining the effect of generator characteristics on the resulting acoustic field, we varied the generator spacing, the generator angle of attack, and the common flow direction between the two generators. These parametric studies were performed on the "best" acoustic case, the O case (Fig. 6b). All of these measurements were taken with the 70-deg delta wings at a 20-deg attack angle (unless otherwise noted). Figure 16 shows that modest variations of generator spacing have little effect on the acoustic field even though those variations appeared visually to alter the mixing characteristics. The closer spacing is slightly less efficient at reducing the jet noise, but the differences are mostly within experimental uncertainty. This implies that the sign and symmetry of the vortex pairs have a much larger effect on the noise distribution than does vortex spacing. The distance between the center of the generators s is normalized by the major diameter of the jet D.

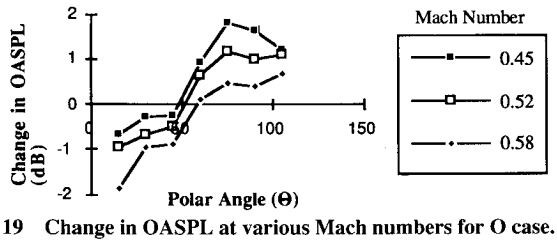

Fig. 19 Change in OASPL at various Mach numbers for O case.

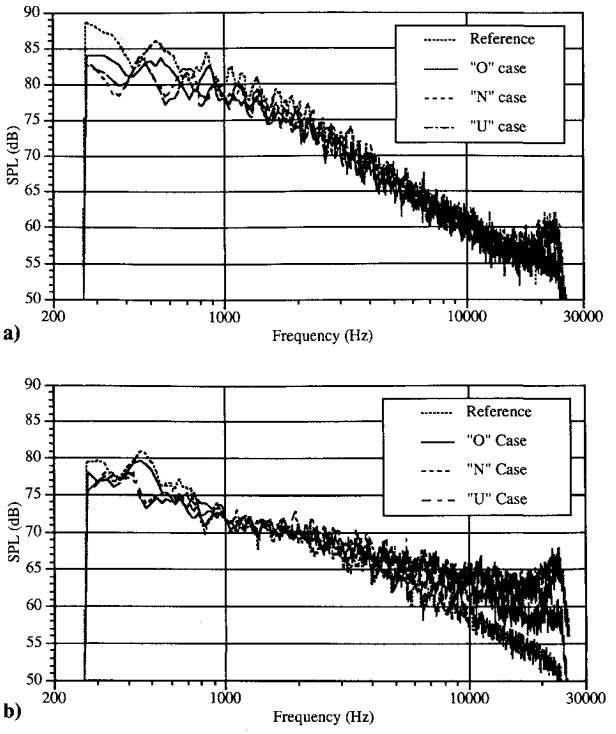

Fig. 20 Comparison of acoustic spectra at a) $\theta = 30$ deg and b) 90 deg ($\phi = 0$, $M = 0.6$).

Figure 17 shows a relationship between the generator angle of attack and the resulting acoustic directivity. The reduction in the overall sound pressure level in the downstream quadrant improves with angle of attack. At an angle of attack of 30 deg, however, we found an increase in the off-axis sound pressure level. Thus, the greater the circulation of the vortex pair, the greater the reduction in on-axis noise. The jump in off-axis noise from the 20 to 30-deg case is interesting and deserves further study.

Figure 18 shows the effect of the direction of the common flow between the two vortices of each vortex pair. The "common flow out" case is identical to the O case; for the "common flow in" case, each generator is rotated so as to produce common flow in at both the top and the bottom of the nozzle. The common flow out case produces a rounder core, whereas the common flow in case tends to split the core into two high-speed regions. With regard to acoustics, the common flow out case decreases the jet noise more than the common flow in case. Although the distance between the vortices (not the generators) is slightly different because of the different generator orientations, the variation in spacing is not sufficient to account for the variation in noise reduction (see Fig. 15). Apparently, from a noise reduction standpoint, moving high-speed fluid away from the jet centerline is more efficient than bringing low-speed fluid toward the centerline.

Figure 19 shows the measured change in OASPL relative to the reference case as a function of jet Mach number. The measurements indicate that the noise reduction increases with jet velocity. This suggests that noise reductions above 3 dB could be achieved at certain polar angles for subsonic flows at $M > 0.6$. This suggests that the extra noise generated directly by the vortices does not increase as strongly with velocity as does the jet low-frequency noise reduction.

Finally, to understand the origin of the noise reduction, one must examine the acoustic spectra. Figure 20 shows a comparison of acoustic spectra for the four cases at polar angles of 30 and 90 deg. Although the spectra clearly show the limitations of the room at low frequencies, one can see that the vortex generators decrease the low-frequency noise but increase the high-frequency noise. At both $\theta = 30$ and 90 deg, the N case generates the most increase in high-frequency noise, and the O case generates the least increase in high-frequency noise, most likely because there are four generators total in the O case and eight in the N and U cases. Since each generator

acts as a noise source, one would expect to see and increase in the high frequencies. Thus, it is not surprising that the O case provides the most overall noise reduction. Because of room limitations, the Sonex walls absorb only 70% of the energy under 250 Hz, and therefore the peak (at about 400 Hz based on the results of Lush[13]) is somewhat obscured. This clouding effect, however, should affect all cases similarly, and therefore the trends in SPL should still be indicative of the far-field behavior. The apparent 300-Hz oscillation in the spectrum is most likely a result of room dynamics. One can show, using the geometry of the room, that sound waves reflecting off the floor will have a path length long enough to generate destructive interference in 360-Hz intervals.

The larger amplitudes of low-frequency noise at $\theta = 30$ deg indicate the well-known directivity of jet mixing noise. Ignoring the artificial increase in low frequency due to the problem with the Sonex walls, one can make out a local peak in the acoustic spectrum at 520 Hz. This corresponds to a Strouhal number based on hydraulic diameter ($St = fd_h/U_0$) of 0.22. For the N and U cases, this local peak shifts down to 450 Hz, indicating perhaps that the streamwise vortices have affected the formation of the primary spanwise structures of the flow.

Concluding Remarks

This study of the effect of streamwise vortices on subsonic rectangular jets clearly shows that streamwise vortices can both enhance mixing and, in some cases, decrease noise. These results are consistent with previous work by several investigators on the influence of vortices produced by tabs. The use of half-delta-wing vortex generators provides direct control of the characteristics of each vortex, and numerous configurations of these generators were considered. Additionally, a simple and efficient optical estimation of mixing effectiveness was presented. Although many improvements can and are being made to this technique for quantifying mixing effectiveness, this technique already provides a useful tool for comparing and evaluating the effectiveness of various vortex generator configurations.

The mixing data indicate that the streamwise vortices improve both large-scale and small-scale mixing. Mass entrainment into the jet increases by up to 50%. Increases in mixing effectiveness and shear layer growth are close to 40% for some configurations. The generator configurations dictate the shape of the jet potential core, and almost any arbitrary shape can be obtained by proper placement of the generators. Flow visualization and mean velocity measurements present consistent images of the jet mixing patterns. Along with changes in shape, the core length also decreases by as much as a factor of 2. The core length, however, is not a good measure of mixing in these highly three-dimensional flows. Integral measures, such as mass entrainment or mixing effectiveness, are more appropriate.

The acoustic results show that streamwise vortices are effective at reducing the overall sound pressure level for polar angles less than 60 deg but increase noise slightly at angles around 90 deg. At all polar angles considered, the streamwise vortices reduce low-frequency noise but increase high-frequency noise. The vortices apparently reduce low-frequency noise by modification of the jet mixing noise sources through a global reduction of the high shear regions of the flow. The increased turbulence associated with the vortices, however, produces the increase in high-frequency noise. The fact that most of the acoustic energy is at lower frequencies for polar angles close to the jet axis accounts for the net reduction in overall jet noise downstream of the jet. To the side of the jet, the increase in high-frequency noise dominates the decrease in low-frequency noise, resulting in an increase in overall jet noise. It should also be noted, however, that the effect of the blockage of the generators would be to decrease the momentum flux, and therefore one would have to have a faster flow exiting the nozzle to have the same momentum flux. The momentum flux difference was less than 5%, implying that the corresponding increase in sound due to this higher velocity would be less than our uncertainty of 1 dB. Finally, the noise reduction increases with both Mach number and generator angle of attack (up to 30 deg).

Acknowledgments

This research was conducted in part under the McDonnell Douglas Independent Research and Development program and in part under Tufts University sponsorship. The authors are grateful to Nat Vignati, Joe Kroutil, Mike Meers, Phil Surks, and Mark Carletti for assisting in these experiments and in the preparation of this manuscript.

References

[1]Ho, C. M., and Gutmark, E., "Vortex Induction and Mass Entrainment in a Small-Aspect-Ratio Elliptic Jet," *Journal of Fluid Mechanics,* Vol. 179, June 1987, pp. 383–405.

[2]Wlezien, R. W., and Kibens, V., "Passive Control of Jets with Indeterminate Origins," AIAA Paper 84-2299, Oct. 1984.

[3]Lee, M., and Reynolds, W. C., "Bifurcating and Blooming Jets," *Fifth Symposium on Turbulent Shear Flows* (New York), Aug. 1985, pp. 1.7–1.12.

[4]Parekh, D. E., Reynolds, W. C., and Mungal, M. G., "Bifurcation of Round Air Jets by Dual-Mode Acoustic Excitation," AIAA Paper 87-0164, Jan. 1987.

[5]Wiltse, J. M., and Glezer, A., "Manipulation of Free Shear Flows Using Piezoelectric Actuators," *Journal of Fluid Mechanics,* Vol. 249, April 1993, pp. 261–285.

[6]Bevilaqua, P. M., "Evaluation of Hypermixing for Thrust Augmenting Ejectors," *Journal of Aircraft,* Vol. 11, No. 6, 1974, pp. 348–354.

[7]Bradbury, L. J. S., and Khadem, A. H., "The Distortion of a Jet by Tabs," *Journal of Fluid Mechanics,* Vol. 70, Pt. 4, Aug. 1975, pp. 801–813.

[8]Ahuja, K. K., and Brown, W. H., "Shear Flow Control by Mechanical Tabs," AIAA Paper 89-0994, March 1989.

[9]Zaman, K. B. M. Q., Reeder, M. F., and Samimy, M., "Supersonic Jet Mixing Enhancement by 'Delta Tabs,'" AIAA Paper 92-3548, July, 1992.

[10]Krishnappa, G., and Csanaday, G. T., "An Experimental Investigation of the Composition of Jet Noise," *Journal of Fluid Mechanics,* Vol. 37, Pt. 1, June 1969, pp. 149–159.

[11]Samimy, M., Reeder, M., and Zaman, K., "Supersonic Jet Mixing Enhancement by Vortex Generators," AIAA Paper 91-2263, June 1991.

[12]Kegelman, J. T., and Roos, F. W., "Effects of Leading-Edge Shape and Vortex Burst on the Flowfield of a 70-Degree-Sweep Delta Wing," AIAA Paper 89-0086, Jan. 1989.

[13]Lush, P. A., "Measurements of Subsonic Jet Noise and Comparison with Theory," *Journal of Fluid Mechanics,* Vol. 46, Pt. 3, April 1971, pp. 477–500.